Supplementary Materials

Evaluating stable isotopic compositions in near-surface atmospheric water vapor over the Tibetan Plateau using the isotope-enabled atmospheric general circulation model ECHAM6-wiso

Yigang Liu[1,2], Jing Gao[1*], Martin Werner[3], Alexandre Cauquoin[4], Ke Li[1,2]

[1]State Key Laboratory of Tibetan Plateau Earth System, Environment and Resources (TPESER), Institute of Tibetan Plateau Research, Chinese Academy of Sciences, Beijing 100101, China

[2]University of Chinese Academy of Sciences, Beijing 100049, China

[3]Alfred Wegener Institute (AWI), Helmholtz Centre for Polar and Marine Sciences, Bremerhaven, Germany

[4]Institute of Industrial Science (IIS), The University of Tokyo, Kashiwa, Japan

[*]Corresponding author: Jing Gao (gaojing@itpcas.ac.cn)

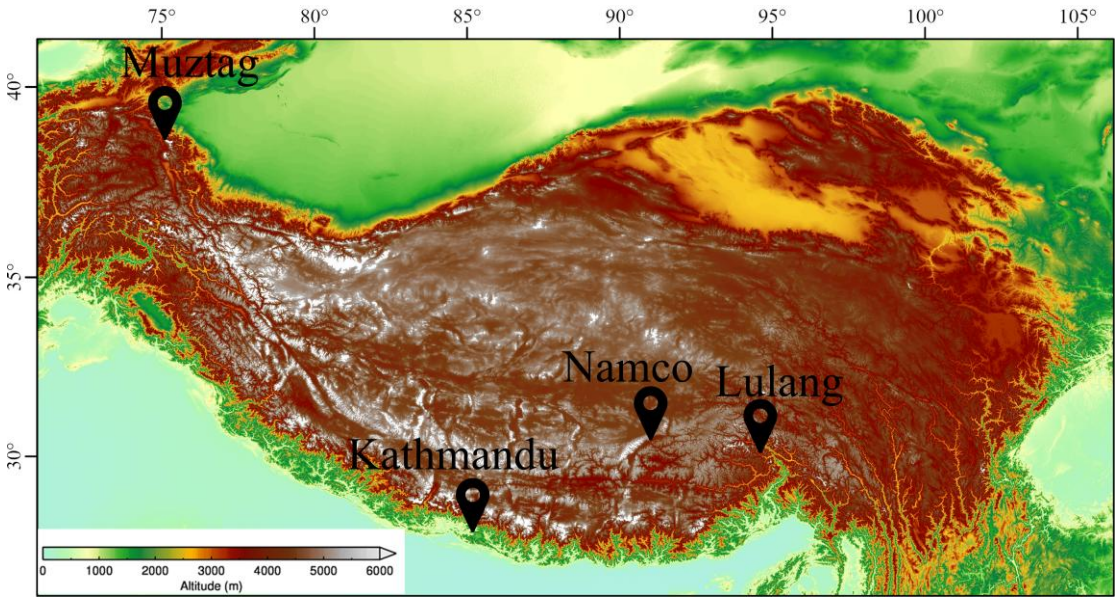

Figure S1. Map of locations for four high-altitude monitoring stations.

Seasonal Cycles of Temperature and Precipitation

Seasonal cycles of temperature and precipitation at four monitoring stations are shown in Supplementary Fig. 1. At Kathmandu site, the maximum precipitation occurred in July that reaching 634.6 mm per month, while in December was the least, to only 1.4 mm/month. The maximum 2 m air temperature occurred in August (19.1 ℃) and reached lowest in January (2.5 ℃). At Lulang site, the maximum precipitation occurred in July (538.6 mm/month), and the minimum precipitation occurred in December (19.4 mm/month). Compared to Kathmandu, precipitation at Lulang shows a more gradual change. The maximum 2 m air temperature occurred in August (9.9 ℃) and reached lowest in January (-7.7 ℃). At Namco site, the station closer to the TP interior, precipitation has sharply decreased. The maximum precipitation occurred in August (93.6 mm/month) and in December was minimum (0.1 mm/month). The maximum 2 m air temperature occurred in July (8.8 ℃) and reached lowest in January (-13.2 ℃). At Muztag site, the only station located in northern TP, presenting the driest characteristics from four monitoring stations. The maximum precipitation occurred in July (58.5 mm/month), and the minimum precipitation occurred in January (17.3 mm/month). The maximum 2 m air temperature occurred in August (9.9 ℃) and reached lowest in January (-15.1 ℃).

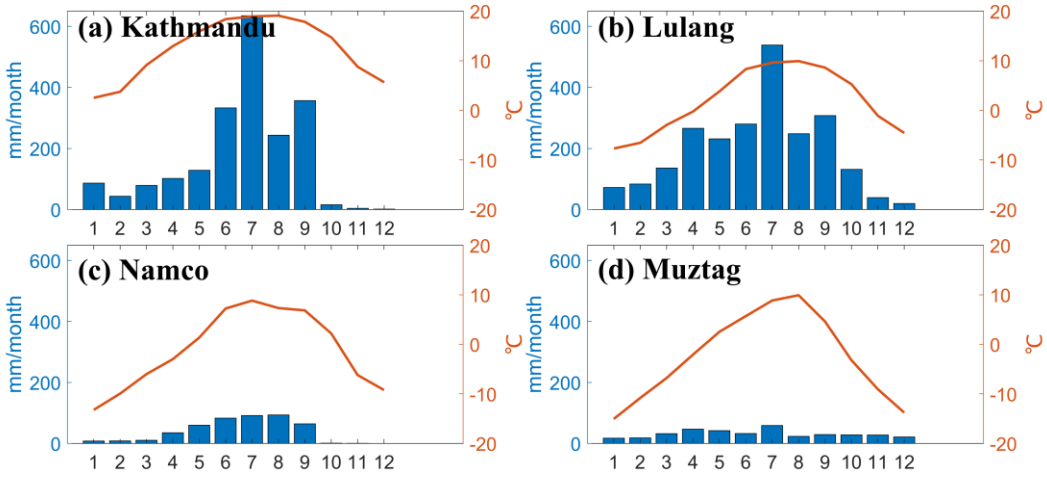

Figure S2. Seasonal cycles of observed 2 m air temperature [℃] and precipitation intensity [mm/month] at (a) Kathmandu, (b) Lulang, (c) Namco, and (d) Muztag.

Results were averaged from year 2020-2021.

Calibration and Quality Control

The observation conditions at four monitoring stations are slightly different. At Kathmandu, Picarro L2130-i analyzer was installed at the Kathmandu Centre for Research Education (KCRE) and the sampling inlet was mounted 7 m above the ground surface with a 10 L min^{-1} pump that deliver air from inlet to the analyzer. Desiccant was used to drying air. At Lulang, ambient air was collected at 2 m above the ground surface, and dry air comes from the external dry air cylinder that is connected. At Namco, the sampling inlets were installed on the flux tower with four different heights (1 m, 4 m, 11 m, 40 m) and switched automatically every 15 minutes. Dry air comes from the external dry air cylinder. At Muztag, the sampling inlet was mounted 2 m above the ground surface, and air was dried through desiccant.

The measured water vapor isotopic ratios from Picarro L2130-i is affected by factors such as humidity (called humidity dependency), and instrument properties (called instrumental drift). Therefore, calibration is necessary to minimize measurement errors as much as possible. Referring Steen-Larsen et al. (2013) and Bastrikov et al. (2014), the calibration protocols are similar across four monitoring stations but slightly different for Namco. Except Namco, standard deliver module (SDM) was used to perform calibration. The SDM controls flow rate of standard to generates standard at different humidity level that covering full range of atmospheric humidity. The calibration protocols including following steps:

1) Humidity dependency calibration: Isotopic values were measured at a constant flow rate of dry air for 25 min at each humidity level and then change gradually. Using a isotopic value that humidity of close to 20,000 ppmv as a true value to calculate differences of measured isotopic value at different humidity levels. Constructing function between different humidity levels and differences to calibrate isotopic observations of the current month. To remove a memory effect, the first 15 min of data from the calculations were excluded.
2) Instrumental drift calibration: two water isotopic standards (S1: $\delta^{18}O$=-10.009‰,

δD=-69.476‰; S2: $\delta^{18}O$=-29.806‰, δD=-227.225‰) were measured at each day with six different humidity levels. Averaging over the last 15 min at each humidity level to obtain a calibrating function by applying regression function to the standards and averaged values.

At Namco, calibration system was replaced with Dew Point Generator (DPG, Steen-Larsen et al., 2014). At each day, the DPG generates two different humidity levels instead of six compared to other stations.

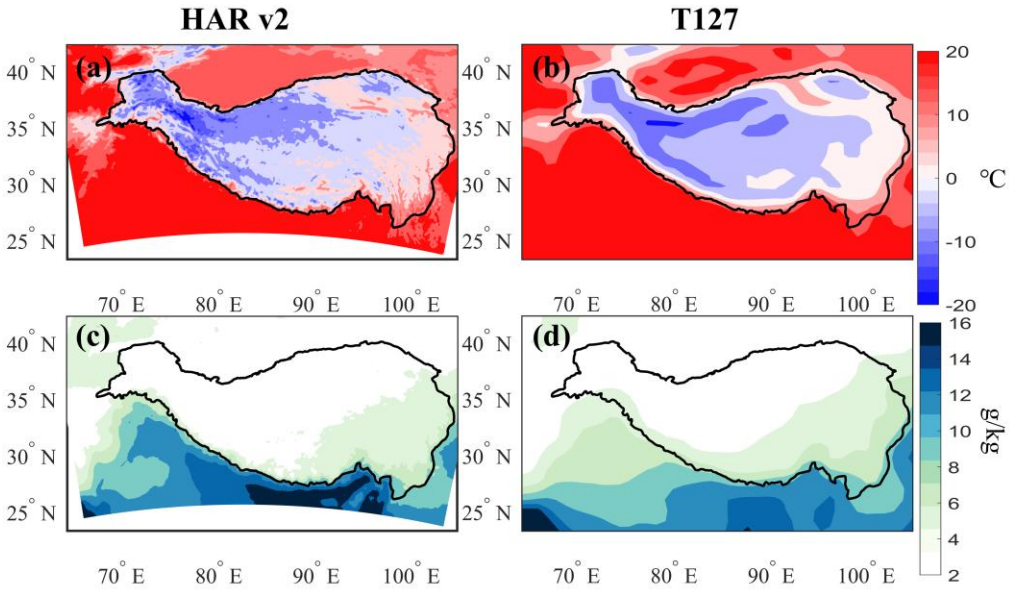

121

122 **Figure S3. Distributions of referenced (HARv2) and simulated (a), (b) 2m air**
123 **temperature [℃] and (c) (d) specific humidity [g/kg], averaged of year 2020-2021.**
124 Black polygon outlines the TP border.

125

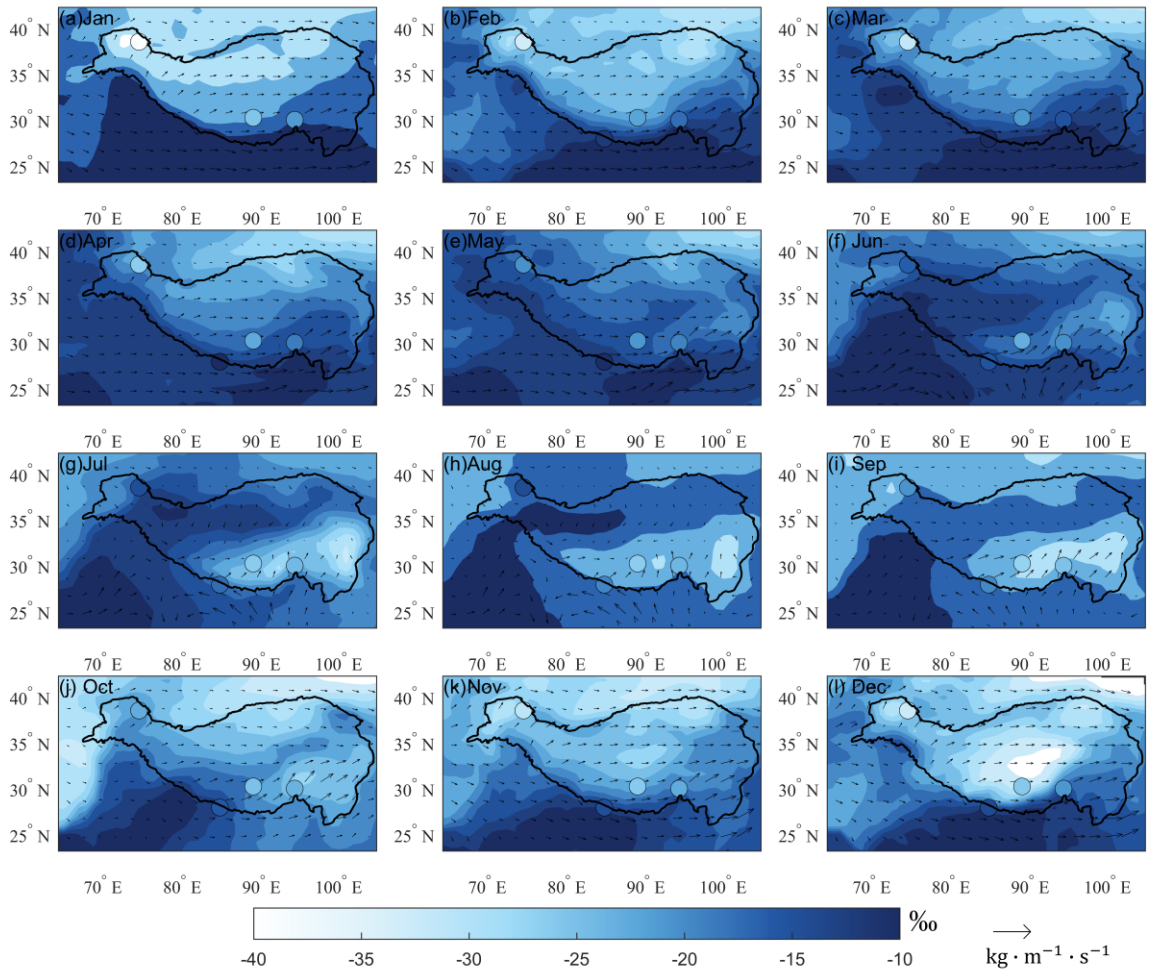

126

127 **Figure S4. Distributions of simulated (colored contours) and observed (colored**
128 **dots) monthly mean near-surface $\delta^{18}O_v$ values [‰], averaged of period 2020-2021.**
129 Black arrows denote the simulated vertically integrated water vapor flux [$kg \cdot m^{-1} \cdot$
130 s^{-1}], while the black polygon outlines the TP border. Note: Panel (a) is missing the
131 observational data from Kathmandu.

132

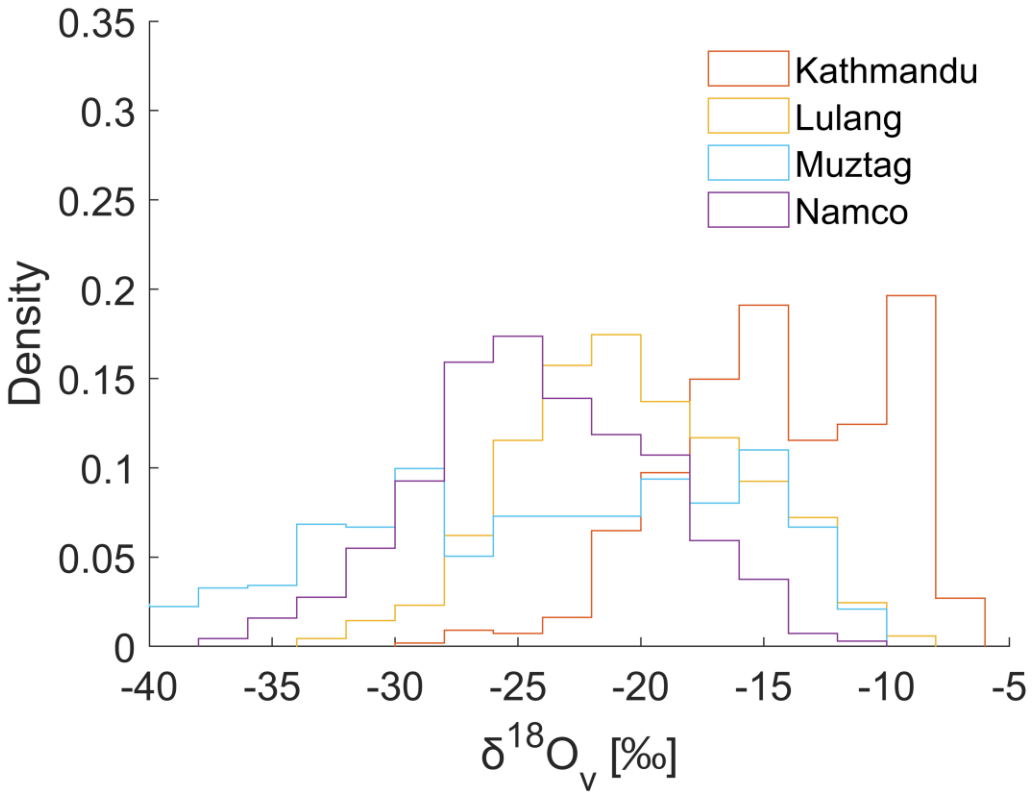

Figure S5. PDFs of observed daily $\delta^{18}O_v$ at Kathmandu (orange), Lulang (yellow), Namco (purple), and Muztag (light blue).

Division for 13 transects over the TP

Given the extremely complex boundaries and variable winds around the TP, it will introduce great uncertainty if only focusing atmospheric moisture transport in four directions. Therefore, it's imperative to demarcate the TP border based on the potential pathways for atmospheric moisture transport. We defined 13 transects attempting to follow the 4000 m a. s. l. in the mountain range and to cut cross the mountain valleys.

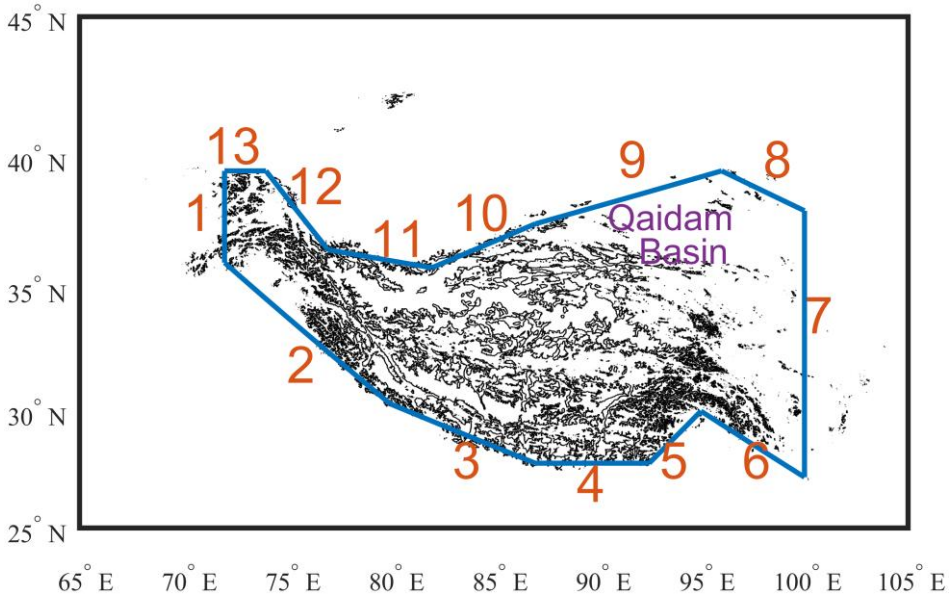

Figure S6. Distribution of the 13 transects (blue lines). Black contours are the elevation of 4000 m a. s. l. over the TP. Length of each transect: transect 1: 389.18 km; transect 2: 1092.30 km; transect 3: 826.52 km; transect 4: 611.57 km; transect 5: 370.30 km; transect 6: 637.22 km; transect 7: 1200.90 km; transect 8: 475.02 km; transect 9: 1025.20 km; transect 10: 587.23 km; transect 11: 561.40 km; transect 12: 471.76 km; transect 13: 222.39 km.

Atmospheric moisture transport

Atmospheric moisture transport is commonly expressed by the water vapor flux in an atmospheric column, which can be calculated as:

$$q_{flux} = \rho \cdot q \cdot v, \quad (1)$$

ρ is the air density ($kg\ m^{-3}$), q denotes the specific humidity ($kg\ kg^{-1}$), and v is the horizonal wind vector ($m\ s^{-1}$).

Total air column water vapor flux is calculated by integrating water vapor fluxes over the whole air column:

$$Q = \int_{p_{surf}}^{p_{top}} \frac{1}{g} \cdot q_{flux}\, dp, \quad (2)$$

where Q is the vertically integrated water vapor flux ($kg \cdot m^{-1} \cdot s^{-1}$), p_{top} and p_{surf} represent the pressure at the top atmosphere and surface, respectively, while g is acceleration by gravity ($9.8\ Pa \cdot m^2 \cdot kg^{-1}$).

Inflow profile

We calculate perpendicular vector values of atmospheric moisture transport relative to the transect as the inflow. Thus:

$$q_{flux,input} = q_{flux} \cdot \sin\theta, \quad (3)$$

where $q_{flux,input}$ is the inflow and θ is the angle between the atmospheric moisture transport and the transect.

inflow profiles can be obtained by calculating the inflow at each atmosphere level along a transect. Ideally, this involves identifying the grid cells that intersect with the transect to derive the inflow profile. However, due to the mismatches between the grid cells and the transect locations, we first identify grid cells within 30 km of the transect. The transect is then discretized into n equally spaced points. For each point, the nearest grid cells are used to calculate the mean inflow. At the junction of the two transects, the overlapping grid cells are used only for the subsequent transect to prevent double counting. This procedure is repeated for each atmosphere level to obtain the inflow profiles.

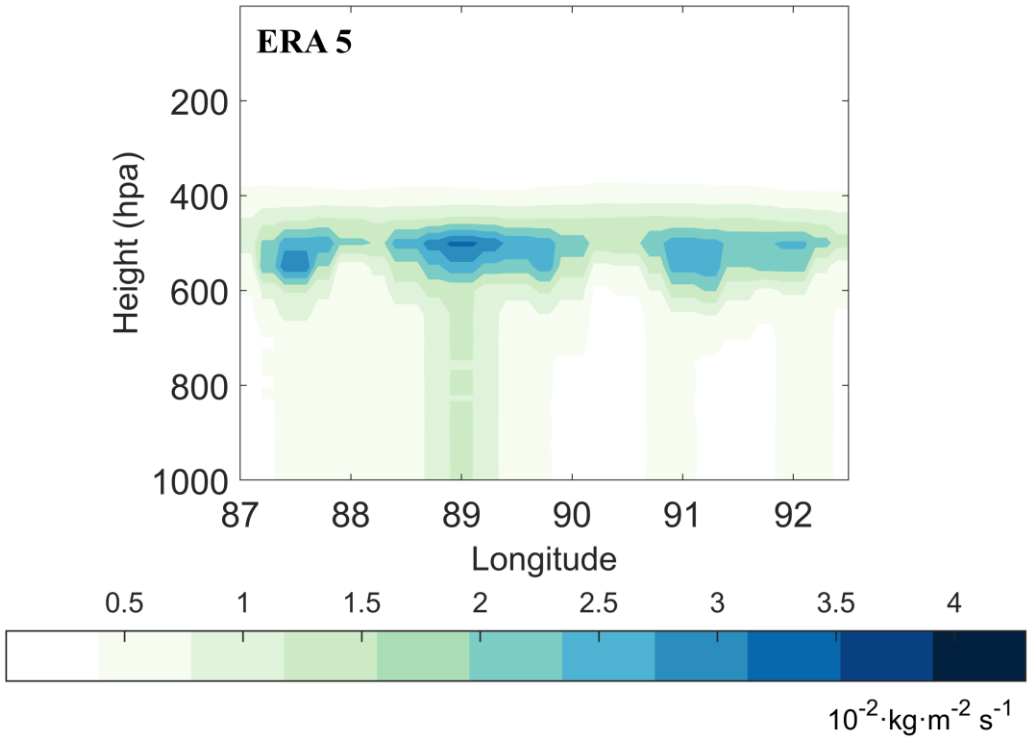

Figure S7. Inflow profile [10^{-2} kg m^{-2} s^{-1}] on transect 4 derived from ERA5.